

Functional forms for photon spectra of clinical linacs

E S M Ali and D W O Rogers

Carleton Laboratory for Radiotherapy Physics, Department of Physics, Carleton University,
1125 Colonel By Drive, Ottawa, ON K1S 5B6, Canada

E-mail: eali@physics.carleton.ca and drogers@physics.carleton.ca

Received 26 May 2011, in final form 18 September 2011

Published 29 November 2011

Online at stacks.iop.org/PMB/57/31

Abstract

Specifying photon spectra of clinical linacs using a functional form is useful for many applications, including virtual source modelling and spectral unfolding from dosimetric measurements such as transmission data or depth-dose curves. In this study, 11 functional forms from the literature are compiled and quantitatively compared. A new function is proposed which offers improvements over existing ones. The proposed function is simple, physics-based and has four free parameters, one of which is the mean incident electron kinetic energy. A comprehensive benchmark set of validated, high-precision Monte Carlo spectra is generated and used to evaluate the strengths and limitations of different functions. The benchmark set has 65 spectra (3.5–30 MV) from Varian, Elekta, Siemens, Tomotherapy, Cyberknife and research linacs. The set includes spectra on- and off-axis from linacs with and without a flattening filter, and in treatment and imaging modes. The proposed function gives the lowest spectral deviations among all functions. It reproduces the energy fluence values in each bin for the benchmark set with a normalized root-mean-square deviation of 1.7%. The mean incident electron kinetic energy, maximum photon energy, most-probable energy and average energy are reproduced, on average, within 1.4%, 4.3%, 3.9% and 0.6% of their true values, respectively. The proposed function is well behaved when used for spectral unfolding from dosimetric data. The contribution of the 511 keV annihilation peak and the energy spread of the incident electron beam can be added as additional free parameters.

(Some figures in this article are in colour only in the electronic version)

1. Introduction

One of the methods to specify photon spectra of clinical linacs is to assume that the spectra follow a certain *functional form* with a few free parameters. Each spectrum is then fully characterized by a unique set of those parameters. This parameterization approach makes the spectra more portable and compact, facilitates virtual source modelling (Fippel *et al* 2003, Sikora *et al* 2007) and tames the classic ill-conditioned problem of unfolding photon spectra from dosimetric measurements such as transmission data (Baker *et al* 1995) or depth-dose curves (Ahnesjö and Andreo 1989), by reducing the task to only finding the free parameters for the spectrum in question. Ideally, a suitable functional form should satisfy the following seven conditions: it should (1) be relatively simple so that its behaviour is easily understood; (2) have reasonably few free parameters for the function to be robust during spectral unfolding; (3) be based on physics to prevent unphysical shapes; (4) be flexible enough to accommodate current clinical spectra of interest (different manufacturers, beam energies, beam modifiers, on- and off-axis spectra, etc); (5) be able to uniquely discern spectra with slight energy variations; (6) clearly characterize the endpoint energy, which has been traditionally difficult to unfold (Baker and Peck 1997); and (7) not require *a priori* knowledge of the spectrum or the linac head. Current treatment planning systems (TPSs) that use semi-analytical dose calculation engines may not have such stringent conditions on the accuracy of the input photon spectra or the functional forms representing them. This is because of the presence of other model approximations and tweaking parameters. However, as TPSs move towards Monte Carlo engines and more detailed patient and beam modelling, the requirements on the spectral functional form become more stringent, particularly for accurate dose calculations around tissue heterogeneities (Charland *et al* 2004). Accurate spectral knowledge is also useful for better modelling of the energy response of detectors in a given beam (Tonkopi *et al* 2005).

We are currently pursuing a project with the goal of accurately and reliably unfolding linac photon spectra from transmission measurements (Ali and Rogers 2011a) and from depth-dose curves (Ali *et al* 2011). A necessary (but not sufficient) prerequisite to achieve this goal is the choice of a functional form that is accurate, flexible and robust. This is presented separately here because of its general utility. In this study, the functional forms available in the literature are compiled. A comprehensive benchmark set of validated, diverse, high-precision Monte Carlo spectra is generated and used to evaluate the strengths and limitations of different functions. A new function is proposed, which offers improvements over existing ones.

2. Methods

2.1. Functional forms from the literature

In this section, a chronological summary of 11 functional forms from the literature is presented. Notation is standardized as defined in table 1, and a summary of the functions is given in table 2. For brevity, functions are called henceforth by their index (first column in table 2). Energy-independent multiplicative terms and overall free scaling factors that appear in the original functions are not reproduced in table 2 because the need for them can be eliminated with proper normalization. On the other hand, we treat the maximum photon energy, E_m , as a free parameter in the functions that contain it, even if the original authors did not intend it as such (thus in our terminology a three-parameter function implies C_1 , C_2 and E_m). This is because in clinical linacs the mean incident electron kinetic energy, E_e , is typically unknown. Using the commercial nominal MV to represent E_m in a functional form can be a gross approximation, e.g., $E_e = 14.7$ and 19.0 MeV for Siemens KD 18 MV and Elekta SL 25 MV beams, respectively

Table 1. Notation adopted in this study.

Symbol	Definition
E	Photon energy.
$\phi(E), \psi(E)$	Respectively, differential photon fluence and energy fluence at E .
n_b	Number of energy bins in a spectrum; $n_b = 100$.
ϕ_b, ψ_b	Respectively, differential fluence and energy fluence for energy bin b of width dE_b .
ψ_{av}	Average energy fluence; $\psi_{av} = \sum_{b=1}^{n_b} \psi_b dE_b / \sum_{b=1}^{n_b} dE_b$.
E_l, E_m	Respectively, lowest and maximum photon energy in $\psi(E)$.
E_e	Mean incident electron kinetic energy in the Monte Carlo simulation that generated the photon spectrum. $E_m = E_e$ for monoenergetic electrons.
E_t	Mean incident electron total energy; $E_t = E_e + m_e c^2$.
E_{mp}	Most-probable energy of $\psi(E)$ for the bremsstrahlung continuum (i.e. excluding the 511 keV annihilation peak if present).
E_{av}	Average energy of the spectrum; $E_{av} = \sum_{b=1}^{n_b} \psi_b dE_b / \sum_{b=1}^{n_b} \phi_b dE_b$.
n_p	Number of free parameters in a functional form (including E_m or E_e if a function has either of them).
C_f	Free parameter f ; C_f s is a set of C_f parameters.
$\% \Delta^s(X)$	For spectrum s , the per cent deviation of fit, f , from truth, t , for quantity X : $= (100/\psi_{av}^{s,t}) \sqrt{(1/n_b) \sum_{b=1}^{n_b} (\psi_b^{s,f} - \psi_b^{s,t})^2}$ for $X = \psi$, $= 100 X^{s,f} / X^{s,t} - 1 $ for $X = E_e, E_m, E_{mp}$ or E_{av} (see the footnote).
n_s	Total number of spectra in the benchmark set; $n_s = 65$.
$\% \Delta(X)$	Overall per cent deviation over the n_s spectra for quantity X : $= (1/n_s) \sum_{s=1}^{n_s} \% \Delta^s(X)$ for $X = \psi, E_e, E_m, E_{mp}$ or E_{av} .
σ	Per cent standard deviation of the electron Gaussian energy spread around E_e .
w_j	Weight of sub-spectrum j with E_e^j (to model the energy spread of incident electrons).
$d\sigma_{br}/dE$	Bremsstrahlung cross-section, differential in photon energy only.
x	An arbitrary depth in the bremsstrahlung target.
Z	Atomic number.
$\mu_X(E)$	Mass attenuation coefficient of material X at energy E .
$\delta(E - E_{511})$	Dirac delta function at the center of the 511 keV energy bin.
dE_{511}	Width of the 511 keV energy bin (user-defined).

Note: the maximum photon energy, E_m , can be larger than the mean incident electron kinetic energy, E_e , because of the energy spread of the incident electron beam in typical clinical linacs. Therefore the fitted endpoint energy is compared with both the true E_e and the true E_m .

(Sheikh-Bagheri and Rogers 2002b). The alternative of using the physically meaningful MV beam quality proposed by LaRiviere (1989) (which is based on $\%dd(10)$) to fix E_m is also not suitable because it depends on the beam modifiers (as it should).

The authors of functions 2, 5, 7, 10 and 11 unfolded or directly fitted the photon fluence, ϕ , while the rest used the energy fluence, ψ . In this study, ψ is used for all functions because it gives more reasonable weight to the higher energy portion of the spectrum, which constitutes a more rigorous test of the functions. For a given energy range, ψ has a smaller range of variation than ϕ and thus graphically reveals discrepancies better. Also, to first order, ψ is more directly proportional to dose than ϕ because the mass energy absorption coefficient for water is relatively flat at megavoltage energies. Some functions are strictly empirical without physics grounds (functions 2, 6, 7, 8, 10 and 11 are ansatzes), while others are based on physics

Table 2. Chronological list of the functional forms analysed in this study. Notation is defined in table 1 and energies are in MeV. Equation numbers from the original publications are listed for ease of cross referencing. See sections 2.1 and 2.2 for details.

Index	Author(s)	Original equation (s)	n_p	Function
1	Dance and Baggerly (1965)	p 38	2	$\psi(E) = (E_m - E) \exp(-C_1 E / E_m)$.
2	Tarasko <i>et al</i> (1988)	2	6	$\psi(E) = (C_1 + C_2 E_m)(E / E_m)^{C_3 + C_4 E_m} (1 - E / E_m)^{C_5}$.
3	Ahnesjö and Andreo (1989)	4	4	$\psi(E) = E \exp(-\mu_{C_2}(E) C_3) \int_0^{C_1} \frac{d\sigma_{\text{eff}}}{dE} _{(x, E'_e)} \exp[-\mu_W(E) (C_1 - x)] dx$.
4	Baker (1993); Baker <i>et al</i> (1995)	5	4	$\psi(E) = \left[\left(1 - \frac{E}{E_t}\right) (\ln \eta - 1) + C_2 \left(\frac{E}{E_t}\right)^2 (\ln \eta - 0.5) \right] \exp(-\mu_W(E) C_1 - C_3 / E)$, $\eta = \left[\left(\frac{m_e c^2 E}{2E_t(E_t - E)}\right)^2 + \left(\frac{\sqrt{Z}}{111}\right)^2 \right]^{-0.5}$.
5	Krmar <i>et al</i> (1993)	8	4	$\psi(E) = \text{equation 3BS(e) in Koch and Motz (1959)} \times \exp(-C_1 / E^{C_2} - C_3 E)$.
6	Bloch and McDonough (1998)	5a,b	2	$\psi(E) = \frac{E}{C_1 C_2}$ for $E \leq C_1$, and $\psi(E) = \frac{1}{C_2} \exp\left(\frac{-(E - C_1)^2}{2C_2^2}\right)$ for $E \geq C_1$.
7	Fippel (1999)	11	3	$\psi(E) = E^{C_1} \exp(-C_2 E)$ for $E_t \leq E \leq E_m$, and $\psi(E) = 0$ elsewhere.
8	Sawchuk (2001)	4	2	$\psi(E) = \sin[\pi(E - E_t) / (E_m - E_t)] \exp[-C_1(E - E_t)]$.
9	Hinson and Bourland (2002)	13	2	$\psi(E) = (E_m - E) \exp(-\mu_X(E) C_1)$.
10	Sikora <i>et al</i> (2007)	1-4	4	$\psi(E) = (1 - e^{-C_1 E})(e^{-C_2 E} - e^{-C_2 E_m}) \exp[-(\mu_{ST}(E_m) - \mu_{ST}(E)) C_3]$, $\mu_{ST}(E) = 0.027(E + 0.16)^{-1.2} + 0.03$.
11	Davidson <i>et al</i> (2008)	1	5	$\psi(E) = E \left[\frac{\sqrt{\frac{E - C_2}{C_3} + \sqrt{\frac{C_3}{E - C_2}}}}{C_1(E - C_2)} \right] \exp \left[-\frac{\left(\sqrt{\frac{E - C_2}{C_3} - \sqrt{\frac{C_3}{E - C_2}}} \right)^2}{2C_1^2} \right] / \left[1 + \exp\left(\frac{E - C_4}{C_5}\right) \right]$, $C_1 > 0, C_2 < E_t, C_3 > 0$.
12	This study	-	4	$\psi(E) = \psi_{\text{thin}}(E) \exp(-\mu_W(E) C_1^2 - \mu_{Al}(E) C_2^2)$, $\psi_{\text{thin}}(E) = \left[1 + C_3 \frac{E}{E_e} + \left(\frac{E}{E_e}\right)^2 \right] \left[\ln\left(\frac{E_e(E_e - E)}{E} + 1.65\right) - 0.5 \right]$.
13	This study (with 511 keV)	-	5	in 12 above, replace $\psi_{\text{thin}}(E)$ with $\psi_{\text{thin}}(E) + C_4 \frac{\delta(E - E_{511})}{dE_{511}}$.
14	This study (with spread around E_e)	-	5	in 12 or 13 above, replace $\psi_{\text{thin}}(E, C_f S, E_e)$ with $\sum_j w_j \psi_{\text{thin}}(E, C_f S, E_e^j)$.

formalisms (functions 1 and 9 are based on the Kramers spectrum (Kramers 1923), functions 4 and 5 are based on the Schiff thin-target spectra (Schiff 1951, Koch and Motz 1959, Desobry and Boyer 1991) and function 3 and the like are based on thick-target spectra). Note that the Kramers spectrum is technically a thick-target spectrum, but because of its simplicity the functions based on it are not grouped with function 3. The following are relevant details about each function in table 2.

Function 1. Dance and Baggerly (1965). The function was proposed to describe measured bremsstrahlung production from fully stopping aluminium and iron targets bombarded with monoenergetic electrons in the energy range of 0.5–3.0 MeV. The term $E_m - E$ is the approximate Kramers thick-target spectrum, which ignores electron scattering and breaks down at relativistic energies (Koch and Motz 1959); thus the exponential term was added to give the function some flexibility. Note that $\psi(E_m) = 0$.

Function 2. Tarasko et al (1988). The function was proposed to describe bremsstrahlung from thick targets as a gamma source in photo-nuclear experiments (e.g. to unfold photo-fission cross-sections). Note that $\psi(E_m) = 0$. For a fixed E_m , we note that the function reduces to $\psi(E) = (E_m - E)^{C_1} E^{C_2}$, up to a scaling factor.

Function 3. Parameterized thick-target formulae, e.g., Ahnesjö and Andreo (1989). Thick-target formulae use reasonable approximations to account for the spreading and slowing down of electrons in the target (Nordell and Brahme 1984, Findlay 1989, Desobry and Boyer 1991). A number of parameterized functional forms which are based on thick-target formulae have been proposed (Ahnesjö and Andreo 1989, Baker 1993, Harrison et al 1993, Garnica-Garza 2008), an example of which is function 3, which was proposed in the context of spectral unfolding from depth-dose curves. In this function, $d\sigma_{br}/dE|_{(x, E'_e)}$ is the bremsstrahlung cross-section for electrons of kinetic energy E'_e , where E'_e is the mean kinetic energy of the electron spectrum at depth x in the target. The free parameters C_1 , C_2 and C_3 represent, respectively, the target thickness, the flattening filter effective atomic number and the flattening filter effective thickness. Parameterized thick-target formulae are not analysed further in this study for the following four reasons: (1) they are heavily tailored, which restricts how they can be parameterized and makes them inflexible to handle diverse spectra of interest or to compensate for some of the underlying thick-target model approximations; (2) their complexity limits their portability and usefulness; (3) although their fit parameters are usually physically meaningful, the spectral fitting/unfolding may not be sensitive to some of those parameters (e.g. C_2 in function 3); and (4) in spectral unfolding from other measurements, the double integration (once for ψ and once for the integrated detector signal) introduces more numerical noise than the single integration used with simpler ψ functions. This is not desirable in ill-conditioned unfolding problems that are noise-driven. It is useful to note that the thick-target model of Findlay (1989) is unique in that it is a closed form. This led us to try to parameterize it. However, the fit results were significantly worse than our simpler proposed function.

Function 4. Baker (1993) and Baker et al (1995). The function was proposed for spectral unfolding from transmission data. Bremsstrahlung photons were assumed to be produced only in the first thin-target layer, and thus the first square bracket is based on the Schiff thin-target spectrum in the forward direction with a photon emission angle of zero. The use of the forward direction was justified by its suitability for good-beam-geometry central-axis transmission measurements. Photons were assumed to be attenuated by the full thickness

of the target as a free parameter, C_1 . This assumption leads to overattenuation of lower energy photons, and so C_2 (expected to be negative) was introduced to add flexibility to compensate for this assumption. Attenuation by beam modifying devices other than the target was accommodated through C_3 . Baker and Peck (1997) used a two-parameter version of function 4 (where C_2 and C_3 were fixed) to experimentally unfold a 6 MV spectrum, including an estimate of E_m . Baker (1993) and Partridge (2000) investigated the effect of replacing $1/E$ in the exponent with $\mu_X(E)$ for a low-Z material and showed that the two functions produce fits of comparable quality.

Function 5. Krmar et al (1993). The function was proposed for spectral unfolding using a hybrid of photo-activation and transmission data. The function is composed of the Schiff thin-target spectrum, integrated over all photon emission angles (equation 3BS(e) in Koch and Motz (1959)) and attenuated by an energy-dependent exponential. Equation 3BS(e) is not reproduced in table 2 for brevity and because the free parameters (aside from E_m) are outside of it. The function has two problems: large correlation among the free parameters in the exponent and strong nonlinearity of the function with respect to C_2 . To make the function usable for spectral unfolding, Krmar et al (1996) set C_3 to zero and fixed C_2 and E_m , effectively reducing it to a one-parameter function.

Function 6. Bloch and McDonough (1998). The function was proposed for spectral unfolding using hybrid beam data measurements. The energy fluence is represented by a linear function of E for $E \leq C_1$, where C_1 is the most-probable energy, and by a Gaussian function with a spread of C_2 for $E \geq C_1$. The parameter C_1 was extracted from transmission measurements, while C_2 was extracted from small-field depth-dose measurements in the buildup region. The function is continuous at $E = C_1$, tails off at high energies, and depends very weakly on E_m through C_2 .

Function 7. Fippel (1999). The function was proposed for use with the Monte Carlo dose calculation engine XVMC. The dependence on E_m is implicit through the limits of the spectrum. The physical significance of the free parameters is that E_{mp} for ϕ is $(C_1 - 1)/C_2$, $E_{av} = C_1/C_2$, and sampling from this function can be done using the standard gamma distribution routines.

Function 8. Sawchuk (2001). The function was used for spectral unfolding from transmission data in the context of using Monte Carlo to carry out the necessary integrations during minimization. We found the function to be sensitive to E_t , the lowest energy used. Note that $\psi(E_m) = 0$.

Function 9. Hinson and Bourland (2002). The function was proposed for spectral unfolding from transmission data. Similar to function 1, it is based on the Kramers spectrum (thus $\psi(E_m) = 0$) attenuated by a flattening filter made up of a known material, X , with its effective thickness as a free parameter. We note that equation (14) of Hinson and Bourland (2002) implies that function 9 represents the energy fluence *folded with the ion chamber energy response (cavity dose per unit energy fluence)*, which has no physical grounds and contradicts the discussion the function was based on.

Function 10. Sikora et al (2007). Sikora et al (2007) noted discrepancies in output factors for very small and very large field sizes in the work of Fippel et al (2003). Among a number of proposed improvements, they proposed function 10 as more realistic than function 7. Unlike function 7, this function has explicit dependence on E_m . The last exponential

represents attenuation in a flattening filter made up of steel, with its effective thickness as a free parameter, C_3 . Note that $\psi(E_m) = 0$.

Function 11. Davidson *et al* (2008). This ‘Fatigue–Fermi’ function was proposed for a versatile source model as an input to a Monte Carlo dose calculation engine. Apart from E at the beginning of the function to convert ϕ into ψ , the first two terms together are the ‘Fatigue life’ distribution encountered in engineering modelling applications (<http://www.itl.nist.gov/div898/handbook/eda/section3/eda366a.htm>), with C_1 called the *shape parameter* (significantly affects the shape), C_2 the *location parameter* (related to the location of the most-probable energy) and C_3 the *scale parameter* (related to the distribution width). Apart from normalization factors, the second term is the probability density function of the standard normal distribution with argument $(\sqrt{(E - C_2)}/C_3 - \sqrt{C_3/(E - C_2)})/C_1$, while the last term is the Fermi density distribution, which brings down the tail near E_m . For robustness, Davidson *et al* (2008) used a four-parameter version in which C_4 and C_5 in the Fermi term (which are related to E_m) were fixed to $0.85 E_m$ and $0.15 E_m$, respectively, making it a four-parameter function.

2.2. Proposed functional form

The function proposed in this study (12–14 in table 2) offers improvements over existing ones in order to meet the conditions outlined in section 1. Similar to function 4, bremsstrahlung photons are assumed to be produced in the first thin-target layer, $\psi_{\text{thin}}(E)$, and then attenuated by two materials representative of the target (high Z) and the aggregate of beam-modifying devices (low/medium Z), with the effective thicknesses of the two materials as free parameters, C_1^2 and C_2^2 , respectively. The use of the square for the two free parameters is to ensure positivity, which we found to be necessary for the robustness of the form when used for spectral unfolding from measured dosimetric data. Testing the quality of fits against the benchmark set of spectra when using different combinations of low- and high- Z materials in the proposed function shows that the $\% \Delta$ metrics (defined in table 1) are insensitive to the exact choice of the two materials, and thus tungsten and aluminium are used. If it is desired to have a self-contained function that does not require reading or interpolating attenuation data, $\mu_W(E)$ and $\mu_{Al}(E)$ can be represented by their parameterized versions given in table 3. Using these expressions instead of the actual μ data has a negligible effect on the quality of spectral fits. Simpler expressions of μ can be used at the expense of spectral fit quality.

Unlike function 4, a thin-target spectrum *integrated over all photon emission angles* is employed for two reasons. First, the angular spread of electrons is much larger than that for the produced photons and can safely be assumed isotropic; therefore, an integral over all *electron angles* (even if one is only interested in their contribution to forward photon production) becomes an integral over *photon emission angles*, as argued by Desobry and Boyer (1991). Second, the function is required to be flexible enough to handle off-axis spectra and spectra averaged over large fields (not just good-beam-geometry central-axis spectra), and thus an all-angle formula is more appropriate. Although an all-angle formula overestimates the photon lower energy component in the forward direction (because in reality lower energy photons are more isotropic than higher energy ones), this overestimation is naturally compensated for in three ways: (1) lower energy photons are overattenuated by the full target thickness because in reality they are produced deeper in the target; (2) they are preferentially eliminated by the flattening filter (if it exists); and (3) the beam softening due to scatter by the target and/or the flattening filter is ignored.

Table 3. Parameterization of $\mu_W(E)$ and $\mu_{Al}(E)$ for possible use in the proposed function. Over the energy ranges shown, the typical local error using the standard NIST energy grid is 0.5%. The lower energy limits correspond to the highest energy characteristic peaks of the respective materials. Below the lower energy limits the parameterization of μ is still smooth but deviates from the true values with insignificant effect on the spectral fit quality.

j	0	1	2	3	4	5
$\mu_W(E) = \exp\left[\frac{\sum_{j=0}^2 a_j E^j}{\sum_{j=0}^3 b_j E^j}\right]$, for $69.5 \text{ keV} \leq E \leq 30 \text{ MeV}$						
a_j	6.575×10^0	-3.623×10^1	-1.578×10^0	–	–	–
b_j	1.000×10^0	9.667×10^0	7.132×10^{-1}	-3.778×10^{-4}	–	–
$\mu_{Al}(E) = \frac{\sum_{j=0}^5 a_j (\ln E)^j}{\sum_{j=0}^5 b_j (\ln E)^j}$, for $1.56 \text{ keV} \leq E \leq 30 \text{ MeV}$						
a_j	6.107×10^{-2}	1.694×10^{-2}	-2.390×10^{-3}	3.116×10^{-4}	5.286×10^{-4}	2.507×10^{-5}
b_j	1.000×10^0	7.769×10^{-1}	2.434×10^{-1}	3.838×10^{-2}	3.042×10^{-3}	9.686×10^{-5}

Using a specific all-angle formula (e.g. equation 3BS(e) as done in function 5) would be unjustifiably restrictive for a function that is phenomenological anyway. Therefore, only the *patterns* that are common to most of the all-angle formulae are extracted. Although the extreme relativistic approximation breaks down at both ends of the spectrum, the discussion below is based on only the thin-target formulae that use this approximation because those that relax it (e.g. equation 3BN in Koch and Motz (1959) or equation (24) in Desobry and Boyer (1991)) are overly complex to parameterize. In tables 1 and 2 of Koch and Motz (1959), apart from physical constants and keeping terminology differences in mind, most of the 3Bx and 3Cx all-angle formulae contain the three terms: 1, $\frac{E_t - E}{E_t}$ and $\left(\frac{E_t - E}{E_t}\right)^2$. The first and third terms almost always have a fixed ratio to each other, while the second is scaled by various constants, approximate screening functions and Coulomb corrections. With simple algebraic manipulation it is justifiable to include the parameterized term $\left[1 + C'_1 \frac{E}{E_t} + \left(\frac{E}{E_t}\right)^2\right]$ in the proposed function. Similarly, the term $\frac{E_t(E_t - E)}{E}$ (a bremsstrahlung impact parameter) appears with various screening functions and Coulomb corrections added to it inside and outside a logarithmic function. Therefore multiplying the square bracket just mentioned by $\left[\ln\left(\frac{E_t(E_t - E)}{E} + C'_3\right) + C'_2\right]$ is reasonable. Our optimization results show that replacing E_t with E_e has virtually no effect on the $\% \Delta$ metrics of fit quality, and it is thus adopted for simplicity, i.e. the function includes $\left[1 + C''_1 \frac{E}{E_e} + \left(\frac{E}{E_e}\right)^2\right] \left[\ln\left(\frac{E_e(E_e - E)}{E} + C''_3\right) + C''_2\right]$. Imposing the physical condition $\psi(E_e) = 0$ requires that $C''_3 = \exp(-C''_2)$. To choose an optimum C''_2 , the proposed function is fit to the benchmark set of spectra for a range of C''_2 values within $[-3.0, 3.0]$ in 0.25 increments. Figure 1 shows that $C''_2 = -0.5$ (and consequently $C''_3 = 1.65$) achieve the lowest $\% \Delta$ metrics; therefore, they are used in the proposed function (function 12 in table 2), and they can be thought of as average nuclear screening and/or Coulomb correction factors.

Positrons are created in pair production events in various linac components; they later annihilate producing a discrete 511 keV peak superposed on the bremsstrahlung continuum. If desired, this 511 keV peak can be modelled in any functional form using a Dirac delta function, $\delta(E - E_{511})$, at the centre of the 511 keV bin with amplitude C_4/dE_{511} , where C_4 is a free parameter representing the *integral* energy fluence contribution of the 511 keV photons, and it is bin-size independent (function 13 in table 2).

Requiring $\psi(E_e)$ to be zero is reasonable. However, the differential bremsstrahlung cross-section at E_e is actually finite (Matthews and Owens 1973). Moreover, in clinical linacs

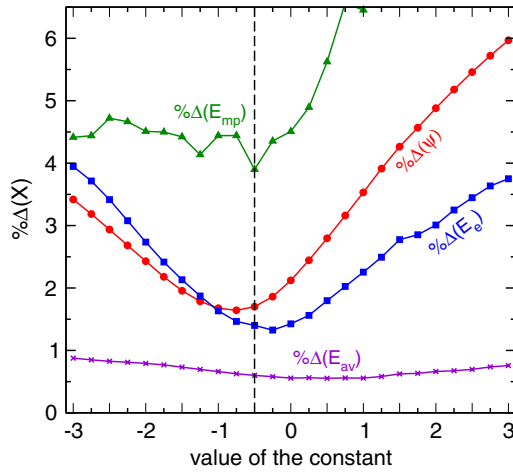


Figure 1. Optimum value of the constant C_2' (discussed in section 2.2) for the proposed function. Notation is defined in table 1.

the incident electron beam has an energy spread that typically varies from a full-width at half-maximum (FWHM) of $\sim 3\%$ (e.g. Varian beams—Cho *et al* (2005)) up to $\sim 20\%$ (e.g. Siemens beams—Sawkey and Faddegon (2009)). These two considerations make the maximum photon energy, E_m , inherently ill defined for typical clinical linac spectra. However, using a function with a clear endpoint energy (e.g. the proposed function) is still preferred over using one that tails off without a definitive E_m (e.g. functions 6, 7 and 11) because it makes unfolding spectra from dosimetric measurements more sensitive to the higher end of the spectrum (Ali and Rogers 2011a). If desired, the energy spread of the incident electron beam can be incorporated into the functional form by replacing $\psi_{\text{thin}}(E, C_{fs}, E_e)$ with $\sum_j w_j \psi_{\text{thin}}(E, C_{fs}, E_e^j)$, where the spectrum is assumed to be composed of a finite number of spectra with different endpoint energies, E_e^j , and weights, w_j . Values of E_e^j s are related to the mean electron energy, E_e , through a parameter representative of the energy spread which can be an additional free parameter if not known (function 14 in table 2). For instance, for Gaussian energy spread with a standard deviation σ , a possible incorporation of the energy spread within 2σ would be $E_e^j = E_e \pm 0.5\sigma$ and $E_e \pm 1.5\sigma$, with w_j (from the standard normal distribution) = 0.34 and 0.16, respectively. The free parameters are then C_{fs} , E_e and σ . This approach is valid for any energy spread that can be characterized with one free parameter (not necessarily Gaussian).

2.3. Benchmark set of spectra

Previous studies either did not validate their proposed functions or they tested them only against spectra which were limited in number, diversity, accuracy, precision and/or energy resolution. This can mask limitations in the functions such as inflexibility or instability. The test spectra also varied among different studies, which precludes meaningful evaluation of the functions against each other. In this study, our benchmark set consists of 65 validated Monte Carlo spectra with high-energy resolution and high statistical precision. The set covers the energy range of interest in radiation therapy (3.5–30 MV). It includes spectra from Varian, Elekta, Siemens, Tomotherapy and Cyberknife machines (with a flattening filter (WFF), flattening-filter free (FFF), on- and off-axis, treatment and imaging modes), and systematic sets of spectra from the research linacs of the National Research Council of Canada (NRC) and the National Physics Laboratory (NPL) in the UK. Off-axis spectra go as far off-axis as clinically relevant

(the periphery of a 40×40 cm² field). The average statistical uncertainty in each bin is a few tenths of a per cent for all spectra except for Tomotherapy (<1%). The following details on how we generated the benchmark set are pertinent.

1. *Varian, Elekta and Siemens spectra.* Sheikh-Bagheri and Rogers (2002a, 2002b) used EGS4 (Nelson *et al* 1985) to model nine common linac beams (Varian Clinac 4 MV and Clinac 2100C/2300C 6, 10, 15 and 18 MV; Elekta SL25 6 and 25 MV; and Siemens KD 6 and 18 MV) using the proprietary specifications from the manufacturers. Incident electron parameters were determined from best fits to generic depth-dose and profile data. In our study, the nine beams WFF are re-simulated with EGSnrc (Kawrakow 2000, Kawrakow and Rogers 2007) for better accuracy and precision. Incident electron parameters are the same as those in the original study (table 1 in Sheikh-Bagheri and Rogers 2002b). The FWHM of the Gaussian energy spread ranges from 3% (Varian) to 17% (Elekta). Within a 40×40 cm² field at 100 cm SSD, on- and off-axis spectra are extracted in, respectively, a 100 cm² central area and a rim between radii of 15 and 20 cm. Each spectrum has 100 equal-size energy bins (bin widths range from 40 to 200 keV, depending on the maximum photon energy of each spectrum).

There is increasing interest in FFF linacs because of their advantages with intensity modulation and small beamlets. In this study, the flattening filters in the nine beams above are removed, and on- and off-axis spectra (defined as above) are extracted. Typically, when the flattening filter is removed a medium-Z plate is added for different reasons. However, its exact material, thickness and position are currently in a state of flux (Georg *et al* 2011). In this study, for the Varian and Elekta 6 MV beams, copper plates of respective thicknesses 2 and 6 mm (Georg *et al* 2011) are placed roughly at the centre of mass of the removed flattening filter. No plate is added for the Siemens 6 MV beam (Siemens, personal communications). In total, 36 clinical spectra are generated (nine beams, WFF, FFF, on- and off-axis).

2. *NRC Vickers spectra.* Faddegon *et al* (1990, 1991) used the NRC Vickers linac to carry out absolute direct measurements of forward and angular bremsstrahlung production from fully stopping thick targets. Pre-target material was minimal and the little post-target material was corrected for. The spectra are useful for the benchmark set because they are accurate, different from typical clinical spectra, and systematically cover a range of beam energies (10–30 MV in 5 MV increments) and targets (beryllium, aluminium and lead). However, they are too noisy to rigorously test the functional forms. Therefore, in this study, we model the original setup with EGSnrc using the details given in Faddegon *et al* (2008) for geometry, materials, revised electron energies (10.09, 15.18, 20.28, 25.38 and 30.45 MeV—independently known using a calibrated bending magnet) and energy spread (Gaussian with 1.5% FWHM). Only the central axis spectra (within a 0.5° cone half-angle) are generated. Each spectrum has between 55 and 110 energy bins of variable size to exactly match those of the measured spectra. Excellent overall agreement is obtained between our Monte Carlo results and the experimental spectra, with beryllium exhibiting the worst agreement (similar to the results in figure 8 of Faddegon *et al* (2008)). In total, 11 central axis spectra are generated: one 15 MV spectrum with a beryllium target and five MV spectra for each of the aluminium and lead targets.

3. *NPL linac spectra.* Walters and Rogers (2000) used EGS4 to model the NPL linac beams and reported good agreement with measurements of %dd(10) and TPR₁₀²⁰. Each beam has two configurations: WFF alone ('light' filtration) and WFF plus 5–14 cm of aluminium filtration ('heavy' filtration). Spectra were averaged over the ~105 cm² central field at ~119 cm SSD. The spectra are useful for our benchmark set because they systematically cover a range of

beam energies (4, 6, 8, 10, 12, 16 and 19 MV) and filtration. In this study, we re-simulate the NPL linac beams with EGSnrc for better accuracy and precision using the details given in Walters and Rogers (2000) for geometry, materials and incident electron parameters (conical beams of monoenergetic electrons with the nominal energy and no energy spread). In total, 14 spectra, each with 100 equal-size energy bins, are generated.

4. *Spectra of dedicated IMRT linacs (Tomotherapy and Cyberknife)*. Jeraj *et al* (2004) used MCNP4c3 (Briesmeister 1999) to model the unflattened beam of a Tomotherapy unit using the exact (and proprietary) mechanical and material specifications. Spectra were reported for the treatment mode and the MVCT imaging mode. The tuned incident electron energies were, respectively, 5.7 and 3.5 MeV, and the energy spread was Gaussian with 12% FWHM ($\sigma = 5\%$). Our benchmark set includes two treatment spectra averaged over $4 \times 5 \text{ cm}^2$ areas at 85 cm SSD and centred at 2.5 and 17.5 cm off axis, respectively, and one imaging spectrum averaged over a central area of $4 \times 40 \text{ cm}^2$ at the same SSD. The spectra (provided by R Jeraj) have between 40 and 70 equal-size energy bins. Araki (2006) used EGSnrc to model the unflattened beam of a Cyberknife unit, with a tuned incident electron energy of 6.7 MeV and a 3% FWHM Gaussian energy spread. Our benchmark set includes the central-axis spectrum (provided by F Araki), which is averaged over a 6 cm diameter area at 80 cm SSD and has 140 equal-size energy bins.

2.4. Fitting

Each function in table 2 is fitted to each spectrum in the benchmark set. The standard Levenberg–Marquardt least-squares minimization algorithm (Press *et al* 1992) is used to minimize $\% \Delta^s(\psi)$ (defined in table 1). Uniform weights for all energy bins are used because the statistical uncertainty on all bins is roughly the same. Analytical first-order derivatives with respect to each free parameter are calculated, and they take the dynamic normalization (through ψ_{av}^s) into account. When a function is highly nonlinear with respect to a parameter, an exhaustive grid search on that parameter is performed while minimizing $\% \Delta^s(\psi)$ with respect to all other parameters. In such a case, the confidence limits on the grid-searched parameter can be estimated using the graphical $\chi_{\min}^2 + 1$ criterion (Rogers 1975). In function 6, C_1 has to be grid-searched because of the discontinuity of $\partial \psi / \partial C_1 |_{E=C_1}$. Functions 2 and 5 exhibit particularly poor robustness because of the large correlation among the free parameters and the strong nonlinearity without an intuitive search domain. In function 8, the quality of fits is sensitive to the value used for E_l (entered manually in this study for each spectrum); this represents a limitation of this function because in a typical spectral unfolding problem the minimum energy is unknown. In function 11, the restriction on C_2 to be smaller than the smallest energy in the spectrum (i.e. $C_2 < E_l$) is not always fulfilled during iterations; this can lead to negative arguments under the square root, which is problematic for unconstrained minimization. Also, the strong nonlinearity of function 11 makes it sensitive to the initial estimates of the free parameters, and expressing C_4 and C_5 as fixed ratios of E_m (section 2.1) does not eliminate this sensitivity. In functions 4, 9 and 12, the XCOM μ values are used (<http://physics.nist.gov/xcom>), with linear interpolation of $\log E$ and $\log \mu$. In functions 9 and 10, respectively, copper and steel (used by the original authors) are used for *all* spectra. Minimization for most functions is virtually instantaneous, but it is slower for functions 5 and 10.

Five $\% \Delta^s$ metrics (defined in table 1) are used to quantify the quality of fit of a function to a given spectrum, s . Since E_m is ill defined for typical clinical linacs (section 2.2), the fitted endpoint energy is compared to both the true E_e (through $\% \Delta^s(E_e)$) and the true E_m

Table 4. Overall quality of fit of different functions to the benchmark set of spectra. Notation is defined in table 1. Parameterized thick-target formulae (function 3 and the like) are not analysed (section 2.1). The ‘robustness’ column qualitatively describes the performance of a function in spectral fitting/unfolding.

Index	Author(s)	n_p	Robustness	$\% \Delta(X)$, X is				
				ψ	E_e	E_m	E_{mp}	E_{av}
1	Dance and Baggerly (1965)	2	Good	27.7	3.9	6.8	69.3	38.4
2	Tarasko <i>et al</i> (1988)	6	Poor	15.2	20.8	16.3	45.4	17.4
3	Ahnesjö and Andreo (1989)	4	–	–	–	–	–	–
4	Baker (1993); Baker <i>et al</i> (1995)	4	Good	2.5	1.9	4.4	9.1	1.2
5	Krmar <i>et al</i> (1993)	4	Poor	2.2	2.8	6.2	3.6	0.8
6	Bloch and McDonough (1998)	2	Fair	13.2	29.7	25.1	40.0	5.9
7	Fippel (1999)	3	Good	18.6	43.9	38.8	32.1	7.3
8	Sawchuk (2001)	2	Fair	27.0	19.6	15.3	62.0	10.7
9	Hinson and Bourland (2002)	2	Good	10.1	5.9	6.1	24.6	3.4
10	Sikora <i>et al</i> (2007)	4	Fair	6.6	6.5	5.0	12.2	5.2
11	Davidson <i>et al</i> (2008)	5	Poor	3.0	7.1	3.4	8.5	0.8
12	This study	4	Good	1.7	1.4	4.3	3.9	0.6
13	This study (with 511 keV)	5	–	1.5	1.4	4.3	3.6	0.6

(through $\% \Delta^s(E_m)$). In functions 6, 7 and 11, the fitted E_m is technically undefined because the functions have indefinite tails. Therefore an arbitrary cutoff (E at which $\psi \approx 3\% \psi_{\text{peak}}$) is used to represent the fitted E_m . The five ‘overall’ $\% \Delta$ metrics (defined in table 1) facilitate quantitative and compact comparison of the functions against each other.

The robustness of the functions when used for spectral unfolding from dosimetric data is qualitatively investigated as follows. Analytical transmission data are generated from known point-source spectra and then smeared multiple times with Gaussian noise typical of a rigorous experimental setup. The noisy transmission data are used to unfold the spectra, and the range of variability in the unfolded spectra is taken as a measure of robustness.

3. Results and discussion

The five overall $\% \Delta$ metrics for the quality of fits of different functions to the benchmark set are shown in table 4. The following observations can be made from the data in the table. The large $\% \Delta$ values for the functions with less than four free parameters (functions 1, 6, 7, 8 and 9) indicate that a truly accurate and flexible function requires at least four free parameters, one of which is the endpoint energy. The proposed function is robust and offers the lowest $\% \Delta$ values, indicating that it is the most accurate and flexible, and thus suitable for use in spectral unfolding problems.

Functions 4, 5 and 11 give the closest $\% \Delta$ values to the proposed function. Therefore some variations of them are considered here as follows. In function 4, when $1/E$ is replaced with $\mu_{Al}(E)$, the five $\% \Delta$ values in table 4 change from (2.5, 1.9, 4.4, 9.1, 1.2) to (2.2, 1.4, 4.4, 7.8, 1.2). In function 5, when C_2 is fixed to an average value, the robustness improves but the quality of fits worsens significantly. Also, in function 5, when the exponential term is replaced with $\exp(-\mu_W(E)C_1 - \mu_{Al}(E)C_2)$, making it a three-parameter function, the robustness improves but the $\% \Delta$ metrics worsen from (2.2, 2.8, 6.2, 3.6, 0.8) to (4.6, 4.6, 7.9, 12.8, 2.4). This indicates that using a specific thin-target formula as given is restrictive

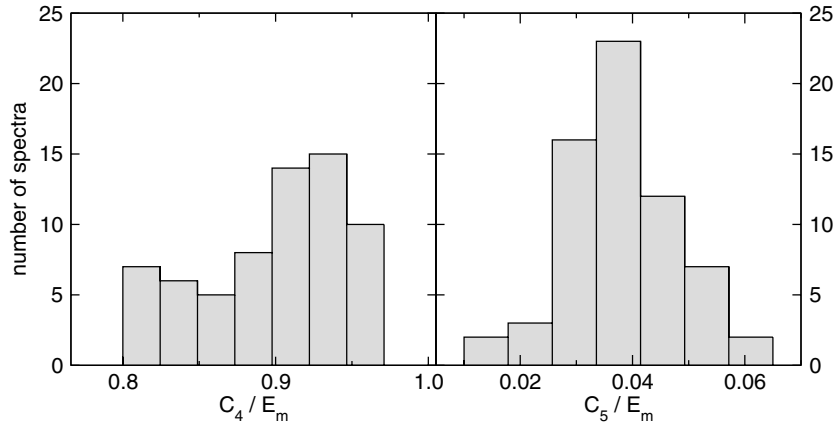


Figure 2. The relation of C_4 and C_5 to E_m in function 11. Values that achieve the best overall performance against the benchmark set of spectra are $C_4 = 0.90 E_m$ and $C_5 = 0.04 E_m$. The values used by the original authors were $C_4 = 0.85 E_m$ and $C_5 = 0.15 E_m$.

for the purpose of parameterization. In function 11, the $\% \Delta$ metrics in table 4 are achieved when both C_4 and C_5 are free parameters and *independent of each other*. When they are fixed to, respectively, $0.85 E_m$ and $0.15 E_m$ (as done by the original authors—section 2.1) and E_m is treated as a fourth free parameter, $\% \Delta(\psi)$ appreciably worsens from 3.0 to 6.9. To better tune the function, we extracted the ratios of C_4 and C_5 to E_m from the free search of the two parameters, as shown in figure 2. The values $C_4 = 0.90 E_m$ and $C_5 = 0.04 E_m$ achieve the best overall $\% \Delta$ values, (3.2, 7.4, 4.2, 8.1, 0.9), which are close to those in table 4, (3.0, 7.1, 3.4, 8.5, 0.8), but with one less free parameter. Based on this discussion and the poor robustness of functions 5 and 11, it can be concluded that function 4 by Baker (1993) offers the second best overall performance.

Examples of the fits of the proposed function (function 13 in table 2) to the benchmark set are shown in figure 3. The fits of that function to the entire benchmark set are available on the web (Ali and Rogers 2011b). Figure 3 demonstrates the overall excellent ability of the function to fit different classes of spectra. Panel (a) shows fits to the spectra of linacs with different head designs. Panel (b) shows fits to the spectra of a given linac beam on- and off-axis, WFF and FFF. Although not obvious in panel (b), the overall quality of fits are marginally better for the central axis spectra than they are for the off-axis ones because the structure of the function is heavily dominated by the forward component. Similarly, fits to the spectra of linacs WFF are marginally better than fits to FFF spectra because the flattening filter reduces the effects of the approximations in the function (section 2.2). Panel (c) shows that for spectra with small electron beam energy spread (3% FWHM for Varian 4 MV), the endpoint energy is fitted accurately, whereas for spectra with large spread (17% FWHM for Elekta 6 MV and 14% FWHM for Siemens 6 MV), the fitted endpoint energy correlates best with the mean incident electron kinetic energy, E_e . This can also be seen in table 4 where the functions that are based on monoenergetic thin-target spectra (functions 4, 5, 12 and 13) have $\% \Delta(E_e) \ll \% \Delta(E_m)$. Panel (d) shows fits to a class of spectra different from typical clinical spectra. The fit of the function to the lead target spectrum is excellent. The fit to the beryllium spectrum is significantly worse than any other fit in the entire benchmark set (with $\% \Delta^s(\psi) = 4.0\%$, while the mean $\% \Delta(\psi)$ when function 13 is fitted to all spectra is 1.5%). It is interesting that the disagreement between the EGSnrc calculations of the beryllium spectrum

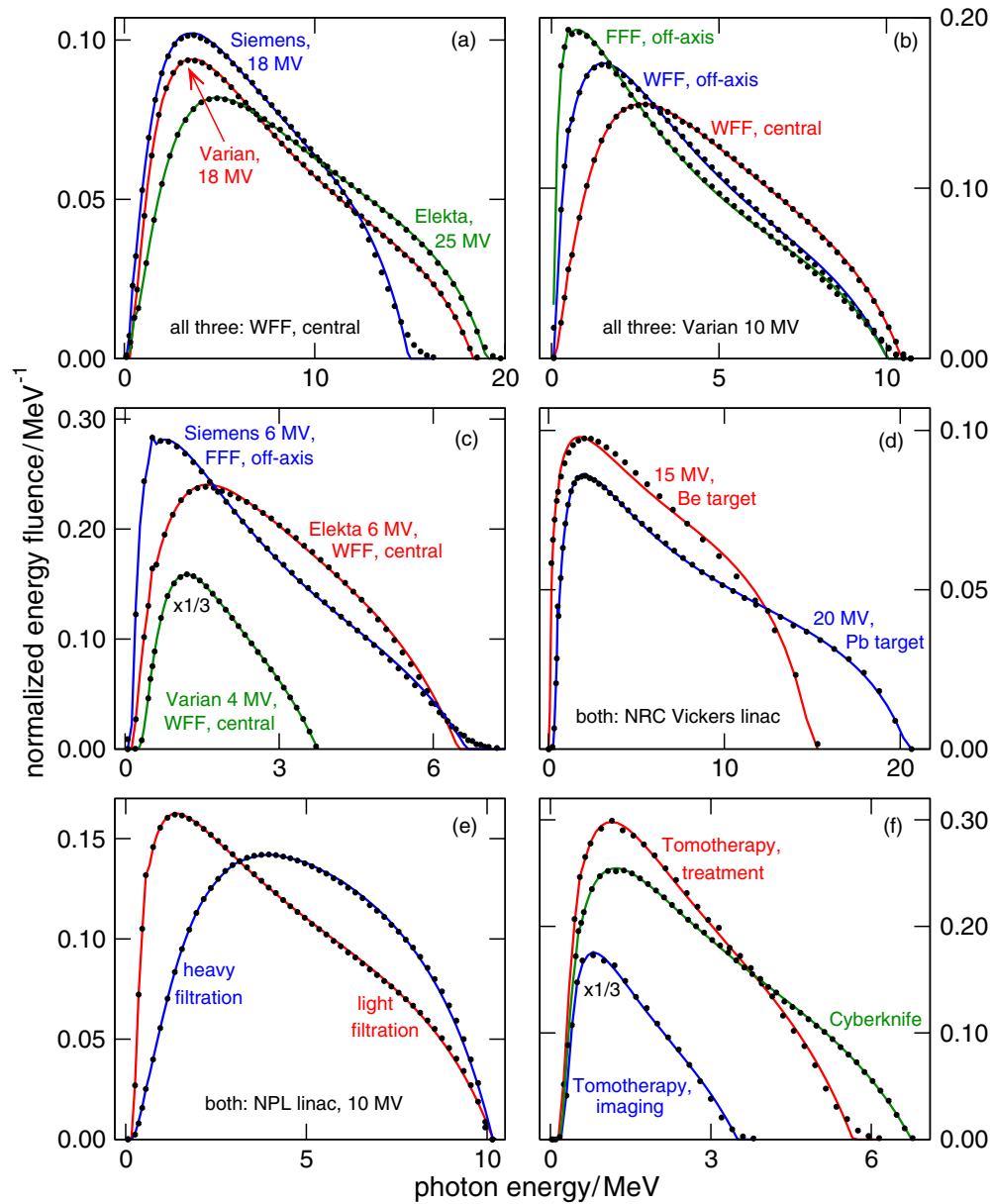


Figure 3. Example fits (solid lines) of the proposed function (function 13 in table 2) to 16 Monte Carlo spectra (dots) from the benchmark set of 65 spectra. The fits are typical of others. The terms ‘central’, ‘off-axis’, ‘WFF’ and ‘FFF’ refer to, respectively, a central-axis spectrum, an off-axis spectrum, with flattening filter and flattening-filter free. For graph clarity, the zero energy is offset, only every other original Monte Carlo point is shown except around the 511 keV peak, and in panels c and f two spectra are scaled down by a factor of 3. Spectra are normalized to unit energy fluence. See section 3 for the significance of the examples in each panel.

and the direct NaI measurements is also larger than it is for the aluminium and lead spectra (section 2.3). Replacing $\mu_W(E)$ in the function with $\mu_{Be}(E)$ does not improve the fit quality. Panel (e) shows excellent flexibility of the function to fit very different spectra created from the same electron beam but with different filtration conditions (14 cm of aluminium added). Panel (f) shows the ability of the function to fit the treatment and imaging spectra of dedicated IMRT machines. In all panels, fits to the 511 keV peak are included, but the peak is visible only in panels (b) and (c).

Examples of the fits of different functions to the benchmark set are shown in figure 4. The following observations can be made using figure 4 and table 4. In panel (a), the fits of function 1 are clearly different from the original spectra, and the function is unable to produce a reasonable inflection point. The $\% \Delta$ values for function 1 are large except for $\% \Delta(E_e)$, which is reasonable because of the condition $\psi(E_m) = 0$. Function 9 is similar in form to function 1, but it performs better because the argument in its exponent is more representative of linac components. In function 8, the quality of fit indicates that a trigonometric function does not provide a particularly good representation of linac spectra. The fit quality with function 8 is significantly worse for softer beams (clinical FFF spectra, off-axis spectra and the Vickers research spectra). In panel (b) of figure 4, function 2 does not produce particularly good fits despite having the largest number of free parameters (with the attendant robustness issues). Also in panel (b), the Gaussian nature of function 6 at the higher end of the spectrum leads to long unrealistic tails (truncated in the graph) and thus to large $\% \Delta(E_m)$ and $\% \Delta(E_e)$ values. Although representing the lower energy part in function 6 by a straight line is generally reasonable, we found empirically that it is problematic when $E_{mp}/E_m < 0.1$ (i.e. softer beams) as seen by the large $\% \Delta(E_{mp})$ value for function 6 in table 4. Panel (c) shows fits of functions 7 and 10 together because the latter was introduced as more realistic than the former (at the expense of an additional fit parameter). Function 7 has long high-energy tails and thus large $\% \Delta(E_m)$ and $\% \Delta(E_e)$ values (similar to function 6 in panel (b)). The effect of the explicit high-energy cutoff in the definition of function 10 is obvious in the fit. Panel (d) shows that the fits of function 4 to the central axis spectra are almost identical to those of the proposed function, but the fits to the off-axis spectra are worse. This is a direct result of the use of a forward-directed thin-target spectrum in function 4 as opposed to the use of the patterns common in thin-target spectra, integrated over all photon emission angles as done in the proposed form. Panel (e) shows that the fits of function 5 are comparable to those of the proposed function, except that function 5 is not robust. When the exponential term is changed to improve robustness, as discussed earlier in this section, the fit quality deteriorates, as shown in panel (e). Panel (f) shows that function 11 matches very well the higher end of the spectra that have large energy spread (the Siemens 6 MV in the panel, with 14% FWHM), whereas the proposed function produces a hard cutoff at an effective E_e . However, function 11 produces the same tail whether or not the original spectrum has it, as shown for the NPL spectrum which has virtually no spread. The quality of fits of function 11 varies among spectra (as seen in panel (f)) and the function typically performs worse for FFF spectra compared with spectra WFF (not shown).

To demonstrate the effect of different spectral fits of a given spectrum on depth-dose curves, EGSnrc is used to calculate central-axis depth-dose curves in a $10 \times 10 \text{ cm}^2$ field for the Varian 6 MV beam WFF using the original spectrum and the fits of all functions. The effect is quantified using the changes in the depth of the maximum dose, d_{\max} , and in the per cent depth dose at 10 cm, $\%dd(10)$, and at 20 cm, $\%dd(20)$. For functions with $\% \Delta(\psi)$ values of only a few per cent (see table 4), d_{\max} remains within 0.5 mm of its true value; the $\%dd(10)$ and $\%dd(20)$ values change by only 0.2% (relative to the maximum dose of 100). For

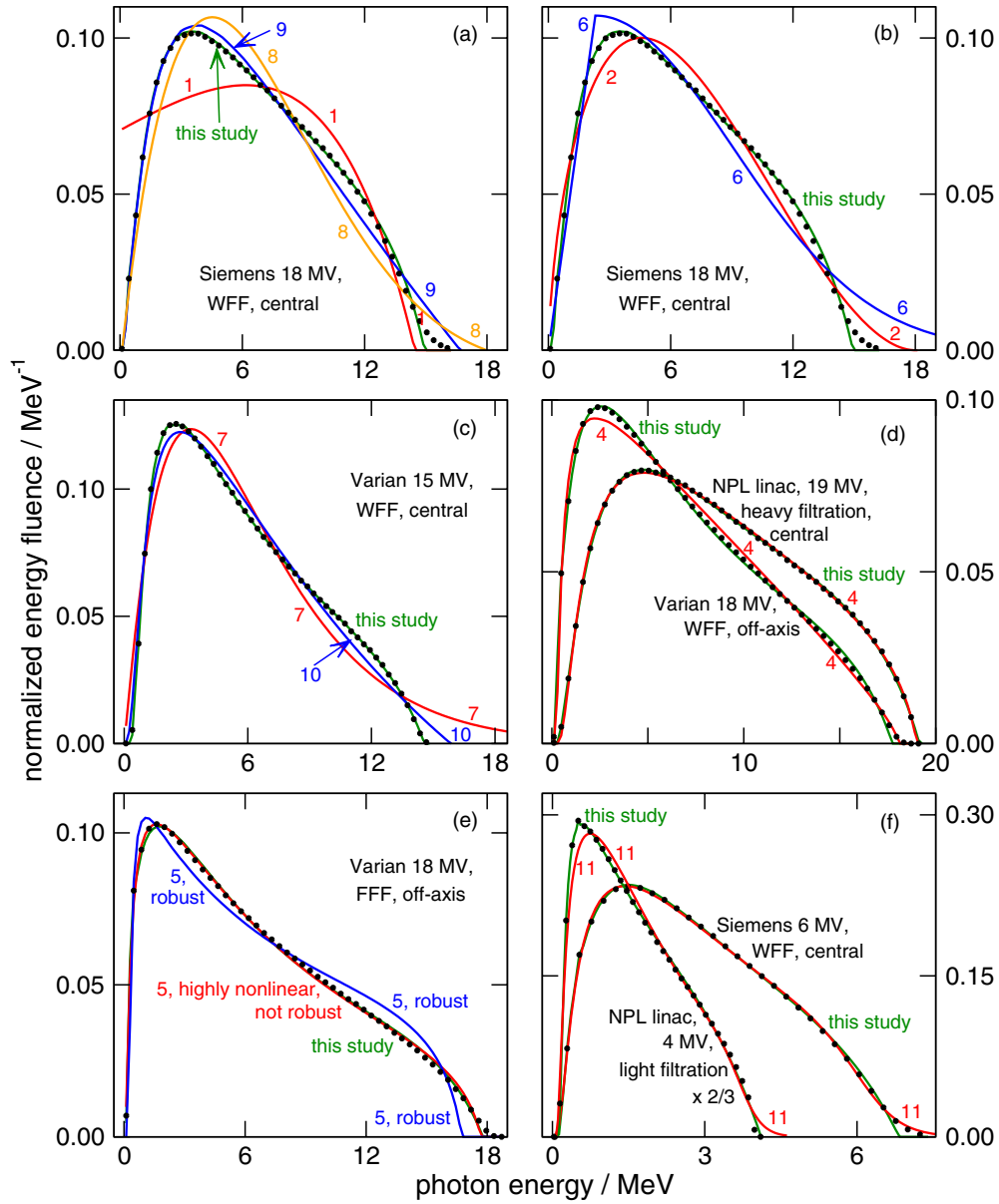


Figure 4. Same as figure 3 but for functions 1 through 11. The fits of the proposed function (function 13 in table 2) are also shown for comparison.

functions with larger $\% \Delta(\psi)$ values, d_{\max} changes by up to 2 mm; the $\%dd(10)$ and $\%dd(20)$ values change by up to 3%.

The largest deviations in spectral fits when using the *simplest* version of the proposed form (function 12 in table 2) are typically for spectra with large electron beam energy spread. For such extreme cases, our EGSnrc calculations of narrow-beam transmission data and depth-dose curves show that d_{\max} remains within 1 mm of its true value, and the values of

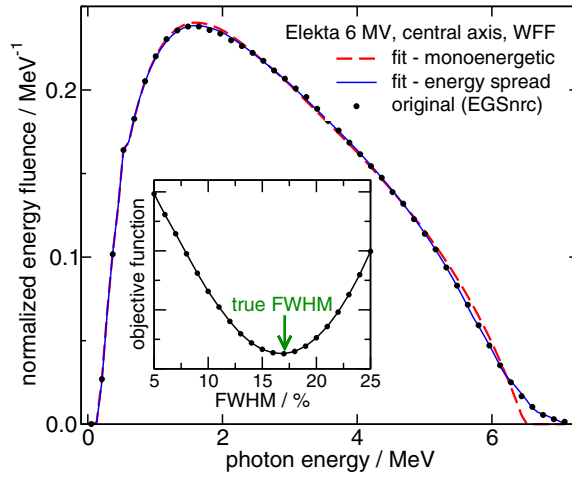


Figure 5. Quality of different fits of the proposed function to a spectrum with a large electron beam energy spread (17% FWHM). The monoenergetic version (function 13 in table 2) and the version that models the energy spread (function 14 in table 2) are shown. The inset demonstrates that the minimization returns the true FWHM value.

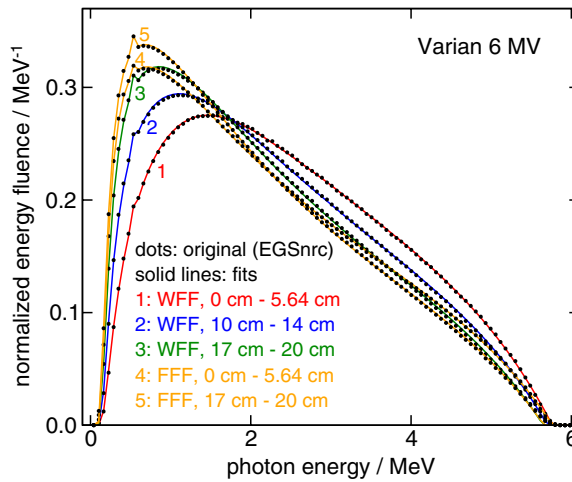


Figure 6. The ability of the proposed function (function 13 in table 2) to model off-axis softening, with and without a flattening filter. The legend gives the radii of the annulus within which each spectrum is obtained from the phase space of a 40×40 cm² field at 100 cm SSD. Spectra are normalized to unit energy fluence.

$\%dd(10)$, $\%dd(20)$ and the smallest transmission signals change by $\sim 0.2\%$. This level of type-B uncertainty is well within the range of the uncertainty of rigorous experiments; therefore, the function can be deemed accurate for spectral unfolding purposes and for representing spectra in dose distribution calculations. If a particular application requires a more stringent representation of the spectrum, then the contribution of the 511 keV annihilation peak and the energy spread of the incident electron beam can be modelled (function 14 in table 2). For instance, when the simple Gaussian model in section 2.2 is applied to the Elekta 6 MV spectrum, and σ (or FWHM) is treated as a free parameter, the minimization returns the true FWHM and the $\% \Delta^s(\psi)$ reduces from 2.4% to 0.6%—see figure 5. Although the

Table 5. Parameters of fitting the proposed functional form (function 13 in table 2) to the energy fluence spectra, $\psi(E)$, generated in this study using EGSnrc for the nine validated linac beams from Sheikh-Bagheri and Rogers (2002a), with their flattening filters present. Notation is defined in table 1. The values given for $C_4 (\times 10^2)$ should be divided by 100 to give C_4 , and they are bin-size independent.

(MV)	C_1 ($\text{g}^{1/2}\text{cm}^{-1}$)	C_2 ($\text{g}^{1/2}\text{cm}^{-1}$)	C_3 –	$C_4(\times 10^2)$ (MeV)	E_e (MeV)	$\%\Delta^s(\psi)$ (%)
Varian Clinac						
4	3.824	3.522	–1.222	0.308	3.75	0.5
6	1.222	5.147	–1.186	0.881	5.76	0.5
10	0.702	6.226	–1.285	3.891	10.46	0.7
15	4.614	3.804	–1.060	14.034	14.58	0.5
18	3.347	5.847	–1.228	43.160	18.33	0.8
Elekta SL25						
6	1.320	5.072	–1.109	2.526	6.49	2.4
25	0.000	7.504	–1.274	57.864	19.02	0.9
Siemens KD						
6	1.184	4.840	–1.161	1.416	6.83	1.9
18	1.213	6.142	–1.126	12.522	14.94	2.2

511 keV contribution and the electron beam energy spread can be extracted from directly fitting the spectrum to the proposed form, they cannot be unfolded as additional free parameters from transmission measurements or depth-dose curves because, as just discussed, their contribution to the measured signals is very small.

Figure 6 demonstrates the excellent ability of the proposed function to model off-axis softening and to model spectra with slight energy variations. All the fit parameters smoothly vary with off-axis distance; therefore, unfortunately, no single free parameter can be used to fully characterize off-axis softening.

There has been a strong interest in the spectra of nine common linac beams modelled by Sheikh-Bagheri and Rogers (2002a) which modelled nine common linac beams. The spectra have been widely used in various dosimetry contexts and they have been recommended by some TPSs (e.g. XiO) as starting spectra for beam modelling. For this reason, the fit parameters for those nine beams WFF, as simulated in this study using EGSnrc, are given in table 5. Except for E_e , the parameters should not be interpreted to represent actual physical quantities.

4. Conclusions

In this study, 11 spectral functional forms from the literature are quantitatively compared using a comprehensive benchmark set of spectra. A new function is proposed which offers improvements over existing ones. It is shown that a truly flexible function requires at least four free parameters, one of which is the endpoint energy. Physics-based functions are preferred because they do not produce unphysical shapes. Parameterizing thick-target formulae is shown to be unnecessary. The four-parameter version of the proposed function reproduces the energy fluence values in each bin for the benchmark set with a normalized root-mean-square deviation of 1.7%. The mean incident electron kinetic energy, maximum photon energy, most-probable energy and average energy are reproduced, on average, within 1.4%, 4.3%, 3.9% and 0.6% of their true values, respectively. The accuracy and robustness of the proposed function make it

suitable for unfolding linac photon spectra from dosimetric measurements such as transmission data or depth-dose curves without requiring *a priori* knowledge of the incident electron beam or the linac head components.

Acknowledgments

We thank Robert Jeraj for the Tomotherapy spectra, Fujio Araki for the Cyberknife spectrum, and Joe Deasy for discussion of function 11. Elsayed Ali acknowledges the funding from a Vanier CGS. Dave Rogers acknowledges the funding from the CRC program, NSERC, CFI and OIT.

References

- Ahnesjö A and Andreo P 1989 Determination of effective bremsstrahlung spectra and electron contamination for photon dose calculations *Phys. Med. Biol.* **34** 1451–64
- Ali E S M, McEwen M R and Rogers D W O 2011 Beyond self-consistency in beam commissioning: determination of true linac spectra *Med. Phys.* **38** 3870–1 (abstract)
- Ali E S M and Rogers D W O 2011a A novel physics-based approach for unfolding megavoltage bremsstrahlung spectra using transmission analysis *Med. Phys.* submitted
- Ali E S M and Rogers D W O 2011b Validation of a new spectral functional form *Technical Report CLRP 11-01* (Ottawa: Carleton Laboratory for Radiotherapy Physics, Carleton University) http://www.physics.carleton.ca/clrp/brem_spectra
- Araki F 2006 Monte Carlo study of a Cyberknife stereotactic radiosurgery system *Med. Phys.* **33** 2955–63
- Baker C R 1993 Reconstruction of clinical bremsstrahlung spectra in the range 4 to 30 MeV *PhD Thesis* University of Surrey
- Baker C R, Ama'ee B and Spyrou N M 1995 Reconstruction of megavoltage photon spectra by attenuation analysis *Phys. Med. Biol.* **40** 529–42
- Baker C R and Peck K K 1997 Reconstruction of 6 MV photon spectra from measured transmission including maximum energy estimation *Phys. Med. Biol.* **42** 2041–51
- Bloch P and McDonough J 1998 Extraction of the photon spectra from measured beam parameters *Med. Phys.* **25** 752–7
- Briesmeister J F 1999 MCNP—a general Monte Carlo *N*-particle transport code, version 4c3 *Los Alamos National Laboratory Report LA-12625* (Los Alamos, NM: Los Alamos National Laboratory)
- Charland P M, Chetty I J, Paniak L D, Bednarz B P and Fraass B A 2004 Enhanced spectral discrimination through the exploitation of interface effects in photon dose data *Med. Phys.* **31** 264–76
- Cho S H, Vassiliou O N, Lee S, Liu H H, Ibbott G S and Mohan R 2005 Reference photon dosimetry data and reference phase space data for the 6 MV photon beam from Varian Clinac 2100 series linear accelerators *Med. Phys.* **32** 137–48
- Dance W E and Baggerly L L 1965 Investigations of electron interactions with matter: part 1. Bremsstrahlung production in aluminum and iron *NASA Report CR-334*
- Davidson S, Cui J, Followill D, Ibbott G and Deasy J 2008 A flexible Monte Carlo tool for patient or phantom specific calculations: comparison with preliminary validation measurements *J. Phys. Conf. Ser.* **102** 012004
- Desobry G E and Boyer A L 1991 Bremsstrahlung review: an analysis of the Schiff spectrum *Med. Phys.* **18** 497–505
- Faddegon B A, Asai M, Perl J, Ross C, Sempau J, Tinslay J and Salvat F 2008 Benchmarking of Monte Carlo simulation of bremsstrahlung from thick targets at radiotherapy energies *Med. Phys.* **35** 4308–17
- Faddegon B A, Ross C K and Rogers D W O 1990 Forward-directed bremsstrahlung of 10 to 30 MeV electrons incident on thick targets of Al and Pb *Med. Phys.* **17** 773–85
- Faddegon B A, Ross C K and Rogers D W O 1991 Angular distribution of bremsstrahlung from 15 MeV electrons incident on thick targets of Be, Al and Pb *Med. Phys.* **18** 727–39
- Findlay D J S 1989 Analytic representation of bremsstrahlung spectra from thick radiators as a function of photon energy and angle *Nucl. Instrum. Methods A* **276** 598–601
- Fippel M 1999 Fast Monte Carlo dose calculation for photon beams based on the VMC electron algorithm *Med. Phys.* **26** 1466–75
- Fippel M, Haryanto F, Dohm O, Nüsslin F and Kriesen S 2003 A virtual photon energy fluence model for Monte Carlo dose calculation *Med. Phys.* **30** 301–11

- Garnica-Garza H M 2008 Determination of radiotherapy x-ray spectra using a screen-film system *Med. Biol. Eng. Comput.* **46** 1029–37
- Georg D, Knöös T and McClean B 2011 Current status and future perspective of flattening filter free photon beams *Med. Phys.* **38** 1280–93
- Harrison R M, Lambert G D and Chapple C L 1993 Spectral estimation and contrast calculation in the design of contrast-detail test objects for radiotherapy portal imaging *Phys. Med. Biol.* **38** 545–56
- Hinson W H and Bourland J D 2002 Spectral reconstruction of high energy photon beams for kernel based dose calculations *Med. Phys.* **29** 1789–96
- Jeraj R, Mackie T R, Balog J, Olivera G, Pearson D, Kapatoes J, Ruchala K and Reckwerdt P 2004 Radiation characteristics of helical tomotherapy *Med. Phys.* **31** 396–404
- Kawrakow I 2000 Accurate condensed history Monte Carlo simulation of electron transport: I. EGSnrc, the new EGS4 version *Med. Phys.* **27** 485–98
- Kawrakow I and Rogers D W O 2007 The EGSnrc Code System: Monte Carlo simulation of electron and photon transport *NRC Technical Report PIRS-701 v4-2-2-5* (Ottawa: National Research Council of Canada), <http://www.irs.inms.nrc.ca/inms/irs/EGSnrc/EGSnrc.html>
- Koch H W and Motz J W 1959 Bremsstrahlung cross-section formulas and related data *Rev. Mod. Phys.* **31** 920–55
- Kramers H A 1923 On the theory of x-ray absorption and of the continuous x-ray spectrum *Phil. Mag.* **46** 836–71
- Krmar M, Slivka J, Bikit I, Vesković M and Čonkić L 1996 Evaluation of bremsstrahlung spectra generated by a 4 MeV linear accelerator *Med. Phys.* **23** 651–4
- Krmar M, Slivka J, Bikit I, Vesković M, Čonkić L, Bistrotić M and Rudić A 1993 A new method for the measurement of bremsstrahlung spectra *Phys. Med. Biol.* **38** 533–44
- LaRiviere P D 1989 The quality of high-energy X-ray beams *Br. J. Radiol.* **62** 473–81
- Matthews J L and Owens R O 1973 Accurate formulae for the calculation of high energy electron bremsstrahlung spectra *Nucl. Instrum. Methods* **111** 157–68
- Nelson W R, Hirayama H and Rogers D W O 1985 The EGS4 code system *Report SLAC-265* (Stanford, CA: Stanford Linear Accelerator Center)
- Nordell B and Brahmé A 1984 Angular distribution and yield from bremsstrahlung targets *Phys. Med. Biol.* **29** 797–810
- Partridge M 2000 Reconstruction of megavoltage photon spectra from electronic portal imager derived transmission measurements *Phys. Med. Biol.* **45** N115–31
- Press W H, Teukolsky S A, Vetterling W T and Flannery B P 1992 *Numerical Recipes in Fortran* 2nd edn (New York: Cambridge University Press)
- Rogers D W O 1975 Analytic and graphical methods for assigning errors to parameters in nonlinear least-squares fitting *Nucl. Instrum. Methods* **127** 253–60
- Sawchuk S 2001 Monte Carlo estimate to improve photon energy spectrum reconstruction *Advanced Monte Carlo for Radiation Physics, Particle Transport Simulation and Applications: Proc. Monte Carlo 2000 Conf. (Lisbon)* ed A Kling, F Barão, M Nakagawa and L Távora (Berlin: Springer) pp 383–8
- Sawkey D L and Faddegon B A 2009 Determination of electron energy, spectral width, and beam divergence at the exit window for clinical megavoltage x-ray beams *Med. Phys.* **36** 698–707
- Schiff L I 1951 Energy-angle distribution of thin target bremsstrahlung *Phys. Rev.* **83** 252–3
- Sheikh-Bagheri D and Rogers D W O 2002a Monte Carlo calculation of nine megavoltage photon beam spectra using the BEAM code *Med. Phys.* **29** 391–402
- Sheikh-Bagheri D and Rogers D W O 2002b Sensitivity of megavoltage photon beam Monte Carlo simulations to electron beam and other parameters *Med. Phys.* **29** 379–90
- Sikora M, Dohm O and Alber M 2007 A virtual photon source model of an Elekta linear accelerator with integrated mini MLC for Monte Carlo based IMRT dose calculation *Phys. Med. Biol.* **52** 4449–63
- Tarasko M Z, Soldatov A S and Rudnikov V E 1988 Description of bremsstrahlung spectra from a thick target for 4–12 MeV electrons *At. Energ.* **65** 290–1
- Tonkopi E, McEwen M, Walters B and Kawrakow I 2005 Influence of ion chamber response on in-air profile measurements in megavoltage photon beams *Med. Phys.* **32** 2918–27
- Walters B R B and Rogers D W O 2000 Monte Carlo estimates of $\%dd(10)_x$ for the NPL photon beams *NRC Report PIRS 659* <http://www.physics.carleton.ca/~drogers/pubs/papers/WR00.pdf>